Engineering Science & Technology
https://ojs.wiserpub.com/index.php/EST/

UNIVERSAL WISER PUBLISHER

Research Article

Modelling Chemical Composition/Temperature Effects on Glass-Reinforced Laterite Bricks via D-Optimal Design

Njuhou Saliou[1*], Cyriaque Rodrigue Kaze[2], Mache Jacques Richard[3], Njindam Oumarou Ramadan[1], Özgur Cengiz[4], Njoya Dayirou[1]

[1]Department of Inorganic Chemistry, Faculty of Sciences, Applied Inorganic Chemistry Laboratory, University of Yaoundé 1, P.O Box: 812, Yaounde, Cameroon
[2]Department of Minerals Engineering, School of Chemical Engineering and Mineral Industries, University of Ngaoundéré, Ngaoundéré, Cameroun
[3]Department of Mining Engineering, School of Geology and Mining Engineering, University of Ngaoundere, P.O. Box: 155 Meiganga, Cameroun
[4]Ceramic Department, Faculty of Fine Arts, Afyon Kocatepe University, 03200, Afyonkarahisar, Turkey
E-mail: njuhousaliou@gmail.com

Received: 14 November 2024; **Revised:** 13 May 2025; **Accepted:** 21 May 2025

Abstract: The effect of SiO_2, Fe_2O_3, ($CaO + Na_2O$), and firing temperature on the characteristics of lateritic clay bricks produced using lateritic clay and recycled waste glass powder was investigated. The mixture was prepared and subjected to firing at 750 and 1,000 °C. The by-products were characterized by their linear shrinkage, flexural strength, porosity, and mineralogy. The flexural strength equation demonstrates a synergistic beneficial interaction between SiO_2 and ($CaO + Na_2O$), which increased the flexural strength, and an antagonistic interaction between Fe_2O_3, ($CaO + Na_2O$), and temperature from 750 to 1,000 °C, which decreased flexural strength by the formation of sillimanite Al_2O_3. In addition, the diffusion process of iron due to temperature led to the substitution of alumina in sillimanite to form $(Al,Fe)_2SiO_5$ and decreased the flexural strength. The linear shrinkage equation demonstrates a synergistic interaction between Fe_2O_3 and temperature, which increased the linear shrinkage. The X-Ray Diffraction (XRD) patterns indicated the presence of hematite, quartz, cristobalite, and sillimanite as the main crystalline phases. The optimal mixture, which meets the desired requirements (porosity ≤ 20%, flexural strength ≥ 4 MPa, and linear shrinkage ≤ 2%), is chemically composed of 34% SiO_2, 37% Fe_2O_3, 14.5% Al_2O_3, 3% ($CaO + Na_2O$), and 10.5% loss on ignition. The corresponding formulation in terms of raw materials is 78% lateritic clay and 22% glass powder, sintered at 888 °C.

Keywords: fluxing oxide, d-optimal design, brick manufacturing, mechanical resistance, shrinkage

1. Introduction

Laterite is widely available in tropical and subtropical regions and covers about 70% of Cameroonian territory [1], [2]. Using lateritic soil in engineering construction projects can result in cost savings. Sandcrete blocks are a key construction material, used extensively in the production of walls for domestic, industrial, and commercial buildings [1]. However, the cost of sandcrete blocks is rising due to the high cost of cement and the growing demand for this material. Compared to standard clayey materials, laterite soils are found on the surface in most cases, which are found at depth,

DOI: https://doi.org/10.37256/est.6220256075

making them less energy-intensive to mine [3]. Several studies were conducted on the use of laterite for the production of fired clay products which developed acceptable performance. The pioneer study was investigated by Mbumbia et al. [1] where the authors used two laterites with different clay content (40-60 wt.%) and heated the samples from 27 to 975 °C. They found that the mechanical strength increased from 2 to 15 MPa and 2 to 13 MPa respectively from samples with high and low clay content. Recently Mbenti et al. [4] produced fired clay products from thermally heated clayey laterites up to 1,050 °C. The high mechanical properties were achieved on samples heated at 950 °C. It was reported a decrease in samples heated at 1,050 °C.

Clay bricks are a widely used construction material due to their mechanical, durability, and thermal performance, as well as their cost-effectiveness [2]. The main factors influencing the properties of clay bricks are typically the raw materials, manufacturing processes, and firing temperature [5]-[7]. Bricks are designed to be strong with homogenous fine pores and a ceramic-like bond developed from the fusion phase of silica and alumina constituents in clay. At high temperatures, clay particles fuse and form a bond with one another [8]. To enhance the bond at low temperatures, additives such as fluxing agents can be incorporated into clay bricks [2], [3]. These additives, which include calcium carbonate sludge (a byproduct of the stone industry), paper mill sludge, arc furnace steel dust, marble residue, sewage sludge, and fly ash, have been utilized in various regions worldwide to improve the sintering properties of clay bricks [9].

The viability of incorporating glass into clay bricks has already been demonstrated [10]-[14]. Several researchers have explored the potential of using glass as a partial substitute for clay in brick manufacturing, to utilize a renewable source [12], [15]. Glass from a variety of sources, including structural glass [15], soda-lime glass [16], electronic devices [17], cathode ray tubes [18], glass sludge from industrial plants [14], and waste colored bottles, can be utilized in brick manufacturing. Dondi et al. [17] demonstrated that the incorporation of glass up to 2% of clay does not result in any notable alterations to the final product. However, an addition of 5% glass led to enhanced mechanical properties. As evidenced in the literature, the addition of glass powder to brick manufacturing generally results in increased mechanical properties, reduced porosity, and decreased linear shrinkage. Consequently, further study of the system glass powder + clays is required, as there is still a need to understand the role played by each oxide and their interactions in that complex mixture.

Ngon Ngon et al. [19] mixed alluvial clay and laterite in proportions of 80/20, 50/50, and 20/80, respectively for the production of fired products between 350 and 1,050 °C. Based on their results samples made with high content of alluvial clay developed flexural strength ranged between 6 and 19 MPa, while those made with less amount ranged between 5 and 16 MPa. Adding alluvial clay as a second aluminosilicate was beneficial for the production of ceramic products with weak porosity. Bodian et al. [20] demonstrated in their study that samples made with 30% laterite and 70% clay developed optimal characteristics such as low shrinkage and high compressive (24 MPa) and flexural strengths (7 MPa), for unfired and fired bricks.

The oxides SiO_2, Fe_2O_3, and ($CaO + Na_2O$) are the main factors that influence the properties of laterite bricks. Their effects and interactions are dependent on their proportion and temperature, making it necessary to conduct an in-depth study on these parameters. Unfortunately, a review of the existing literature reveals a lack of studies investigating the effects and interactions of these oxides on the properties of laterite bricks. Consequently, the objective of this study is to model how the interaction between the initial chemical composition and firing temperature affects the properties of glass-reinforced bricks.

2.Experiments

Figure 1 presents the flowchart of the whole process. More details are provided in the following section.

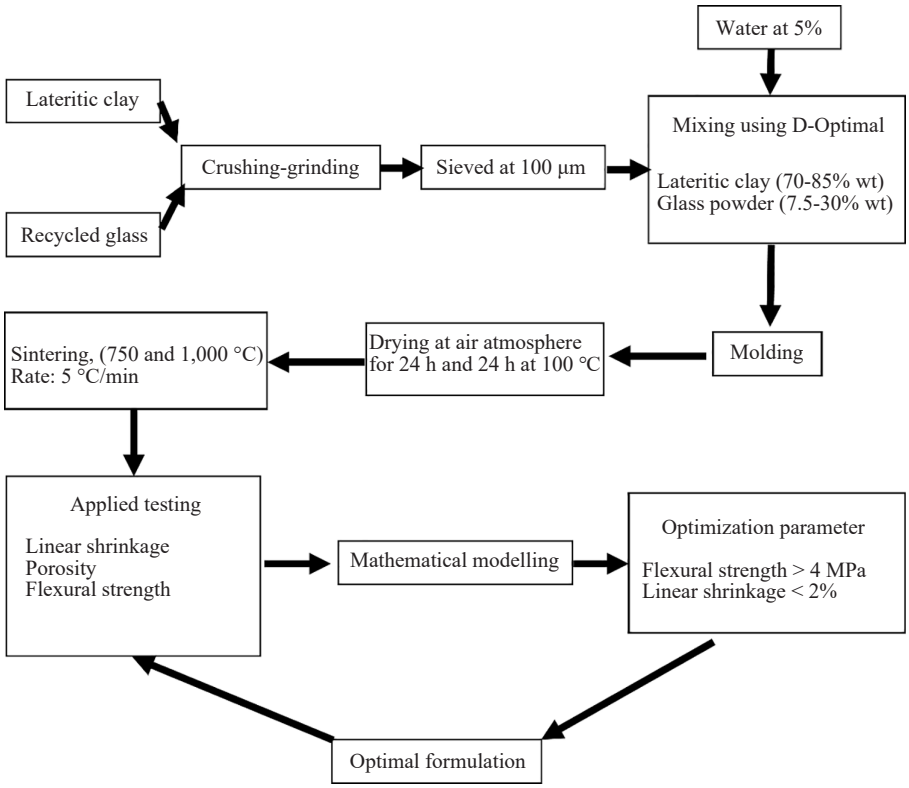

Figure 1. Flowchart of the whole experimental process

2.1 *Raw materials preparation*

The glass waste was initially washed and crushed into small pieces. It was then ground using a ball mill for 1 hour operating at a rotation speed of 100 rpm. Subsequently, the powder was sieved through a 100 µm mesh sieve to produce Glass Powder (GP). The waste glass used in this process is of the soda-lime type.

Subsequently, the lateritic clay (L) was purified and dried in an oven at 100 °C for 24 hours to remove all moisture. Subsequently, the material was crushed in a ball mill for four hours and also sieved at 100 µm. Subsequently, the aforementioned powders (L and GP) underwent X-ray fluorescence (XRF) analysis, conducted using a Bruker S8 Tiger spectrometer.

2.2 *Lateritic bricks formulation and elaboration*

Table 1. Mixtures of lateritic clay (L) and glass powder (GP)

	Percentage of raw materials (%)	
Mixture	Lateritic clay (L)	Glass powder (GP)
F1	85	15
F2	70	30
F3	92.5	7.5
F4	77.5	22.5

The formulations were developed by the Mixture Design methodology, with the process variables evaluated using the Minitab 19 software [21]-[22]. The process variable used in this case is temperature (T), as it is recognized as a crucial process parameter influencing the product characteristics [6], [10]. The temperature was set at 750 and 1,000 °C. To streamline the process and reduce the number of experiments, a D-optimal design based on various percentages of lateritic clay (70-85% w/w) and glass powder (7.5-30% w/w) was employed. The four resulting formulations are presented in Table 1.

The raw materials were mixed in a small porcelain mortar and humidified with 10% distilled water. A rectangular mold with dimensions of 40 × 40 × 80 mm was utilized to shape bricks through uniaxial pressing at a pressure of 12 MPa. A total of five test specimens were produced for each formulation, with an individual weight of 70 grams. Following the pressing process, the samples were initially dried at room temperature for 48 hours, then in an oven at 105 °C for 24 hours. They were subsequently sintered in a Nabertherm furnace (Nabertherm, Grmbh, Lilienthal, Germany).

During the firing process, the temperature was increased at a rate of 5 °C per minute from room temperature to the consolidation temperature (750 °C or 1,000 °C), with a holding period of one hour. Subsequently, the furnace was allowed to cool naturally before the samples were removed.

2.3 *Characterizations*

2.3.1 *Water absorption and porosity*

To ascertain the water absorption rate, the bricks were boiled in distilled water for two hours and then left to stand at room temperature in the same distilled water for 24 hours. The water absorption was calculated using the following equation 1 [23]:

$$w_a(\%) = \frac{M_f - M_i}{M_i} \times 100. \tag{1}$$

M_i is the initial mass of the bricks and M_f is their masses after immersion in distilled water. Porosities π (%) were deduced from water absorption by using equation 2 [12]:

$$\pi(\%) = \frac{M_f - M_i}{V} \times 100. \tag{2}$$

In which, V is the volume of the brick.

2.3.2 *Flexural strength and linear shrinkage*

Flexural strength (σ) tests were conducted on parallelepiped test bars using the three-point bending method with the M & O, type 11.50, NO° 21 machine. The flexural strength was calculated by the methodology outlined in equation 3 below [12]:

$$\sigma = \frac{3FL}{2le^2}, \tag{3}$$

where σ is the flexural strength (MPa), F is the charge applied on the test bar in Newton (N), L is the distance between the two extremities of the test bar, which is a constant (L = 40 mm), l is the material width (l = 40 mm), and e is the material thickness ($e \approx 8$ mm).

The linear shrinkage was determined by direct measurement of the specimen's lengths before and after the firing process. It is crucial for industrialists to control shrinkage, as it can impact the product's shape and dimensions. On the one hand, shrinkage should not cause shape distortions. On the other hand, it must result in final dimensions that closely align with the desired specifications.

2.3.3 *XRD analysis*

The X-ray patterns were recorded using a Philips PW 1729 diffractometer, operating at 40 kV and 40 mA, and using monochromatic CuKα radiation. The X-ray patterns were analyzed using X'Pert HighScore Plus software for mineral identification and semi-quantitative analysis through the Rietveld method. The phase identification and peak and profile data identification methods were employed for the purpose of identifying the phases present. The diffraction files used were Power Diffraction File (PDF)-2 and Crystallographic Open Database (COD).

2.4 *Mathematical modelling*

The general regression models $E[y(x, z)]$ for the combined quadratic model for q mixture components and m process variables with interaction can be expressed in an easily interpretable form as [24], [25]:

$$E[y(x,z)] = \sum_{i=1}^{q} \gamma_i^0 X_i + \sum\sum_{i<j}^{q} \gamma_{ij}^0 X_i X_j + \sum_{l=1}^{m} \left[\sum_{i=1}^{q} \gamma_i^1 X_i + \sum\sum_{i<j}^{q} \gamma_{ij}^1 X_i X_j \right] Z_l + \sum\sum_{l<p}^{m} \left[\sum_{i=1}^{q} \gamma_i^{lp} X_i + \sum\sum_{i<j}^{q} \gamma_{ij}^{lp} X_i X_j \right] Z_l Z_p. \quad (4)$$

Where X_i, $i = 1, \ldots, q$ are the q mixture components; Z_l, $l = 1, \ldots, m$ are m process variables; γ_i^0 and $\gamma_{ij}^0 i, j = 1, \ldots, q$ are the parameters of mixture components; γ_i^1 and γ_{ij}^1 are parameters of mixture experiments associated with process variables Z_l, $l = 1, \ldots, m$ and γ_i^{lp} and γ_{ij}^{lp} are parameters of mixture experiments associated with interaction of process variables $Z_l Z_p$, $l, p = 1, \ldots, m$.

This study considers three mixture constituents ($q = 3$), namely SiO_2, Fe_2O_3, and ($CaO + Na_2O$) oxides. There is only one process variable ($m = 1$), which is the temperature T of the firing process.

Only the response (porosity, flexural strength, and linear shrinkage) with significant variation will be modelled. The regression method will retain only the most statistically significant terms of this general model for each response. The Minitab 19 software was used to create a linear regression model based on the least squares method, which was then used to analyze the experimental data [26]. To assess the significance of the regression models, we employed Analysis of Variance (ANOVA), model adjustment, and prediction coefficients Q^2.

2.5 *Optimization objectives*

The objective of the multi-criteria optimization was to identify a formulation that would enable us to achieve the following specifications: porosity $\pi \leq 20\%$, flexural strength $\sigma \geq 4$ MPa, and linear shrinkage $\leq 2\%$.

A high porosity in bricks leads to a high tendency to absorb water, which is not suitable for bricks. This can result in the development of cracks in the brick body, which will reduce the durability of the product [2].

3. Results and discussion

3.1 *Chemical and mineralogical composition of raw materials*

Table 2 illustrates the chemical composition of the lateritic clay, which is primarily composed of SiO_2 (20%), Al_2O_3 (18%) and Fe_2O_3 (45%). Typically, clay with a SiO_2 content of 50%-60% and an Al_2O_3 content of 10% to 20% is deemed suitable for brick production [2]. This lateritic clay has an adequate quantity of Al_2O_3 for brick manufacturing. The inclusion of an appropriate quantity of SiO_2 enables the attainment of superior mechanical properties and habitually enhances refractory properties by reducing firing shrinkage, plasticity, and drying issues. It is a relatively hard and chemically inert oxide that retains its properties during the firing process. While the selected lateritic clay does not have the requisite amount of silica (50 to 60%) for brick manufacturing, it does have a significant amount of Fe_2O_3 (47%) as fluxes, exceeding 9%. A material with a fluxing agent content exceeding 9% is classified as low refractory [2]. Therefore, this clay is classified as a low-refractory lateritic clay. The CaO percentage (0.05%), which is below the 6% threshold, indicates that this clay is not calcareous [2]. The Crystallographic Open Database (COD) 2021 and the International Centre for Diffraction Data (ICDD) were used to identify all the crystallographic phases in the diffraction

patterns. The lateritic clay is composed of approximately 18% kaolinite ($Al_2O_3 \cdot 2SiO_2 \cdot 4H_2O$) of COD N° 00-029-1488, 23% quartz (SiO_2) of COD N° 01-085-0794, 52% goethite (FeO(OH)) of ICDD 00-029-0713, 3% anatase (TiO_2) of COD N° 00-021-1272, and 4% amorphous phase as estimated by the Rietveld method and illustrated in Figure 2.

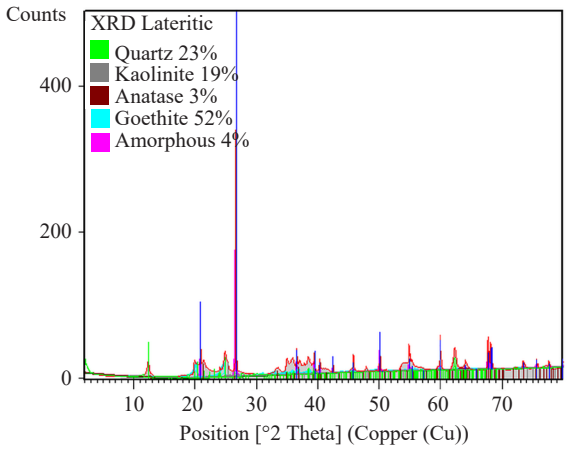

Figure 2. XRD pattern and Rietveld analysis results of lateritic clay (L)

Table 2. Chemical composition of raw materials (%)

Laterite (L)													
SiO_2	Al_2O_3	Fe_2O_3	TiO_2	P_2O_5	Cr_2O_3	MnO	ZrO_2	SO_3	CaO	Cl	K_2O	LOI	Total
20.41	18.15	47.07	0.88	0.29	0.26	0.19	0.08	0.06	0.05	0.05	0.04	12.48	99.96
Glass powder (GP)													
SiO_2	Al_2O_3	Na_2O	CaO	MgO	K_2O	Fe_2O_3	P_2O_5	Cr_2O_3	TiO_2	Cl	SO_3	LOI	Total
68.95	1.75	13.04	10.19	0.84	0.55	0.35	0.02	0.14	0.12	0.07	0.08	3.91	100.0

LOI: Loss of Ignition

Table 3. Chemical composition of each formulation (%)

Formulation	SiO_2	Fe_2O_3	(CaO + Na_2O)	Al_2O_3	LOI
F1	31	40	3.5	16	9.5
F2	38	33	7	18	4
F3	28	44	2	17	9
F4	34	37	5	15	9

LOI: Loss of Ignition

The glass powder contains a high proportion of amorphous SiO_2 (68.95%) and a low proportion of Al_2O_3 (1.75%). The total alkaline flux (CaO + Na_2O) of 23.5% is also suitable for lowering the melting point, should the need arise. The remaining fluxes (Fe_2O_3, MgO, etc.) have a negligible percentage.

The objective of this study is to demonstrate the effect of quartz (SiO_2), alumina (Al_2O_3), iron oxide (Fe_2O_3), and the combined oxides of calcium (CaO), and sodium (Na_2O) on brick properties. Based on the data in Table 1 and the

chemical analysis results in Table 2, the main oxide percentages in each formulation were calculated and are presented in Table 3.

3.2 *Product characteristics*

3.2.1 *Flexural strength and linear shrinkage*

Table 4 illustrates that firing shrinkage ranged from 1.27 to 1.87% at 750 °C and from 4.30 to 6.94% at 1,000 °C. Therefore, the objective of linear shrinkage of no more than 2% has been met for all formulations at 750 °C. The flexural strength (σ) exhibited a range of 0.61 to 2.15 MPa at 750 °C and 2.23 to 6.28 MPa at 1,000 °C. The objective of achieving flexural strength of at least 4 MPa was only met at 1,000 °C. The porosity (π) remains relatively consistent at both temperatures.

Table 4. Experimental results obtained for these formulations

Formulations	Firing shrinkage (%)		Flexural strength (MPa)		Porosity (%)	
	750 °C	1,000 °C	750 °C	1,000 °C	750 °C	1,000 °C
F1	1.58	4.30	1.15	3.24	0.12	0.11
F2	1.27	5.79	2.15	6.28	0.13	0.09
F3	1.87	6.94	0.61	2.23	0.12	0.08
F4	1.82	5.66	1.11	4.23	0.13	0.10

Apart from the porosity, there is no product that combines the desired requirements concerning flexural strength and linear shrinkage (flexural strength $\sigma \geq 4$ MPa and linear shrinkage $\leq 2\%$). To achieve these objectives, it is essential to understand and quantify the impact of the primary oxide, the effects of firing temperature, and the potential interactions between chemical components and temperature on product characteristics.

3.2.2 *XRD results*

The XRD results demonstrate that the primary minerals formed during the firing process are hematite (Fe_2O_3) [COD N° 9015065], quartz (SiO_2) [COD N° 01-085-0794], and two types of sillimanite. The two various types of sillimanite was sillimanite $(Al,Fe)_2SiO_5$ with iron [COD N° 9000994] that has substitute silicium and normal sillimanite (Al_2SiO_5) [COD N° 9003986]. Additionally, other mineral phases were identified, including cristobalite (SiO_2) [ICDD 00-039-1425], rutile (TiO_2) [ICDD 00-021-1276], brownmillerite ($Ca_2(Al,Fe)O_5$) [ICDD 00-030-0226], aluminum titanate (Al_2TiO_5) [ICDD 00-026-0040], wollastonite ($CaSiO_3$) [COD cart N° 9011452], grossular ferrian ($Ca_3(Fe,Al)_2(SiO_4)_3$) [ICDD 00-034-0192], and maghemite (Fe_2O_3) [ICDD 00-039-1346]. These crystalline phases were identified as minor phases. The formation of these diverse phases is attributable to the firing conditions (temperature, pressure, and firing rate), the complexity, and the heterogeneity of the mixtures, which collectively preclude the possibility of selective formation. The various oxides react with one another, resulting in the formation of different minerals.

3.3 *Modelling results and multi-criteria optimization*

3.3.1 *Regression models, variance and coefficient analysis*

The generated regression models are as follows:
Flexural strength:

$$\sigma(\mathrm{MPa}) = -0.073\mathrm{SiO_2} + 0.08\mathrm{Fe_2O_3} - 2.30\left(\mathrm{CaO} + \mathrm{Na_2O}\right) + 0.003\mathrm{SiO_2} \cdot \left(\mathrm{CaO} + \mathrm{Na_2O}\right)$$

$$\left(\mathrm{SiO_2} - \left(\mathrm{CaO_2} + \mathrm{Na_2O}\right)\right) - 0.09\mathrm{Fe_2O_3}\left(\mathrm{CaO} + \mathrm{Na_2O}\right) \cdot T.$$

Linear Shrinkage:

$$LS(\%) = -0.41\mathrm{SiO_2} + 0.31\mathrm{Fe_2O_3} + 1.01\left(\mathrm{CaO} + \mathrm{Na_2O}\right) + 0.05\mathrm{Fe_2O_3} \cdot T.$$

In these equations, SiO_2, Fe_2O_3, and (CaO + Na_2O) respectively represent the percentage of the corresponding oxide in the mixture. T is the firing temperature.

The analysis of variance of the models in Table 5 indicates that all the *P*-values are below the level of significance (α = 0.05) [27]. The flexural strength model yielded a *P*-value of 0.000, while the firing shrinkage model returned a *P*-value of 0.004. Therefore, at least one coefficient for each model is not equal to zero. Therefore, both the flexural strength and linear shrinkage models contribute to explaining and describing the observed variations in responses [28]. Furthermore, the correlation coefficients R^2 are both above 90%. As a result, these models align well with the experimental data. The prediction coefficient is consistently above 80% for flexural strength, which demonstrates the model's high predictive accuracy. With regard to the linear shrinkage, the predicted shrinkage is 71.74, which is deemed sufficient for accurate forecasting.

Table 5. Analysis of variance, correlation (R^2), and prediction (Q^2) coefficient

Response	Variation source	DF	SS	MSS	*F*-ratio	*P*-value	R^2 (%)	Q^2 (%)
Flexural strength	Model	4	25.13	6.28	150	0.000	99.95	99.51
	Residual	3	0.01	0.004				
	Total	7	25.14					
Linear shrinkage	Model	3	34.55	34.55	25.86	0.004	95.10	71.74
	Residual	4	1.78	1.78				
	Total	7	36.33					

Where DF is the Degree of Freedom, SS is the Sum of Square, and MSS is the Mean Sum of Squares

Table 6. Significance of terms for flexural strength

Terms	Estimator	*t*-obs	*p*-value
Quartz	-0.073	*	*
Fe_2O_3	0.08	*	*
(CaO + K_2O)	-2.30	*	*
SiO_2·(CaO + K_2O)(SiO_2 − (CaO + K_2O))	0.003	-8.80	0.003
Fe_2O_3·(CaO + Na_2O)·T	0.009	63.46	0.000

(* means that the term is highly significant)

Tables 6 and 7 show that all regression coefficients have a *p*-value lower than 0.05. All the individual factors (SiO_2, Fe_2O_3, and (CaO + Na_2O)) are highly significant because their *p*-values are strictly null. The *p*-value of interactions in

flexural strength are 0.003 and 0.000 respectively for $SiO_2 \cdot (CaO + Na_2O)(SiO_2 - (CaO + Na_2O))$ and $Fe_2O_3 \cdot (CaO + Na_2O) \cdot T$ interactions. For the linear shrinkage, the *p*-value of $Fe_2O_3 \cdot T$ is 0.001. In conclusion, all the individuals and interaction terms are significant for these models [26].

Table 7. Significance of terms for linear shrinkage

Terms	Estimator	*t*-obs	*p*-value
Quartz	-0.41	*	*
Fe_2O_3	0.31	*	*
$(CaO + K_2O)$	1.01	*	*
$Fe_2O_3 \cdot T$	0.05	8.53	0.001

(* mean that the term is highly significant)

Thus, these models have significant interaction terms. In this case, the effect of each oxide is directly correlated with other oxides or temperature and cannot be interpreted without taking into account the concerned interaction.

3.3.2 *Oxide interactions*

The flexural strength equation demonstrates a beneficial interaction between SiO_2 and $(CaO + Na_2O)$ with a synergistic effect ($0.003 > 0$). Synergistic interactions occur when the combined effect of two or more variables exceeds the sum of their individual effects, resulting in an amplified response. From a chemical standpoint, this interaction can be attributed to the disruption of Si-O-Si bonds in quartz by $(CaO + Na_2O)$ oxides. This resulted in the formation of wollastonite ($CaSiO_3$) and sodium silicate (Na_2SiO_3). The XRD patterns of some formulations (F_2 and F_3 at 1,000 °C) revealed the presence of wollastonite ($CaSiO_3$), as illustrated in Figure 3. The Na_2SiO_3 was not observed in the different XRD patterns. The $(CaO + Na_2O)$ can allow SiO_2 to interact with alumina to form this form of sillimanite (Al_2SiO_5) without iron substituting for aluminum. This is how the interaction between SiO_2 and $(CaO + Na_2O)$ can be synergistic. This model suggests that the formation of sillimanite Al_2SiO_5 without iron as the substituent of some Aluminum atoms increases the flexural strength. The interaction between SiO_2 and Al_2O_3 is not included in the model, as alumina was maintained at a relatively constant level (~17%) across all mixtures.

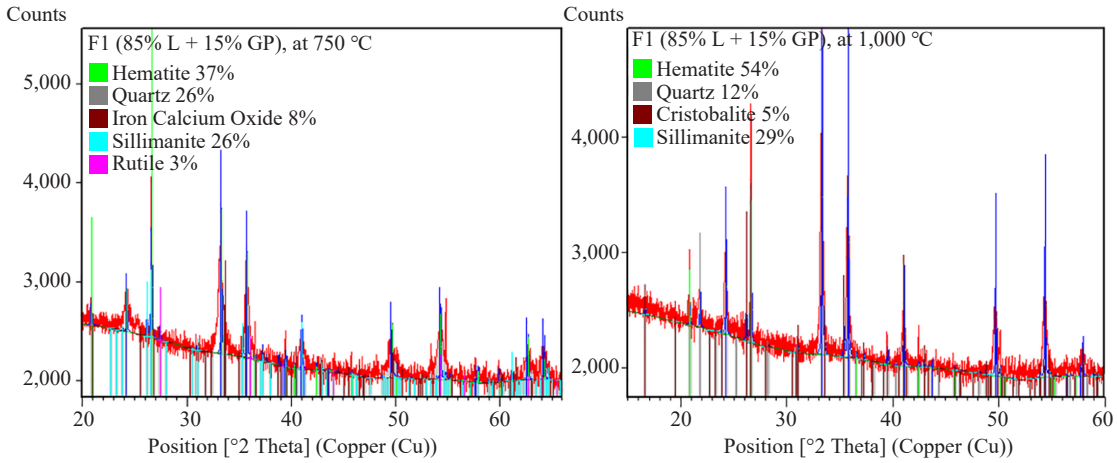

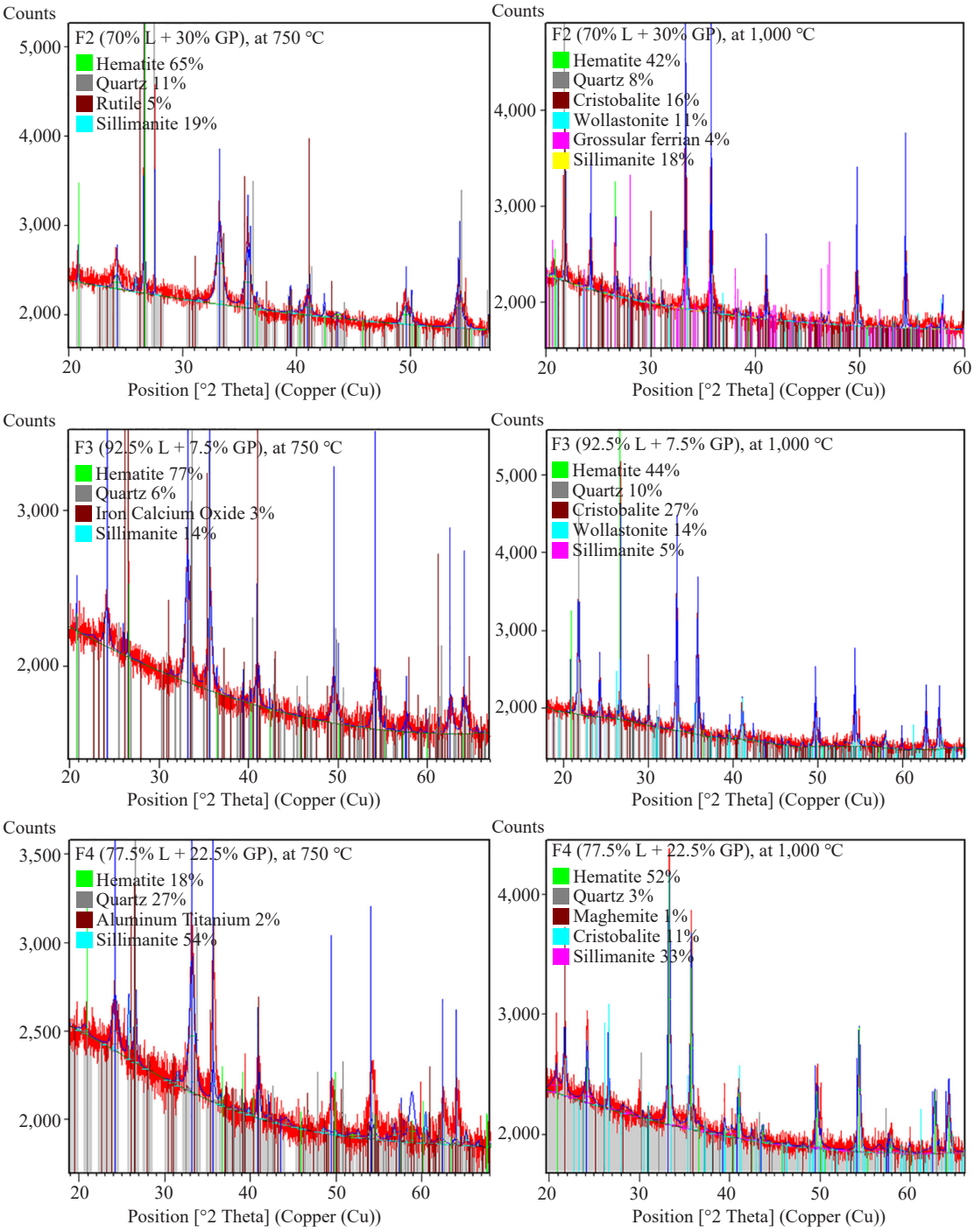

Figure 3. XRD patterns and Rietveld analysis results of formulations

The model demonstrates that temperature interacts with Fe_2O_3 and ($CaO + Na_2O$) in an antagonistic ($-0.09 < 0$) manner. Antagonistic interactions occur when the combined effect of two or more variables is less than the sum of their individual effects, resulting in a diminished response [26]. Therefore, it can be concluded that Fe_2O_3 interacts chemically with ($CaO + Na_2O$) in response to the thermal energy provided by temperature. These interactions have the potential to result in the formation of calcium ferrate ($Ca_xFe_yO_z$) and sodium ferrate ($Ca_xFe_yO_z$), with the values of x, y, and z dependent on the CaO/Fe_2O_3 and Na_2O/Fe_2O_3 ratios. The XRD patterns did not indicate the presence of these compounds. It is likely that this is due to their role as an intermediate in the formation of sillimanite with iron content

$(Al,Fe)_2SiO_5$, brownmillerite ($Ca_2(Al,Fe)O_5$), and grossular ferrian ($Ca_3(Fe,Al)_2(SiO_4)_3$). Consequently, the formation of these compounds may result in a reduction in flexural strength.

Furthermore, the impact of temperature is not linked to SiO_2. This is due to the fact that SiO_2 is chemically stable within the specified temperature range. However, temperature affects the interaction between Fe_2O_3 and ($CaO + Na_2O$), which in turn influences the flexural strength of the fired clay bricks. This is due to the fact that these oxides contribute to the formation of a liquid phase during firing, according to the sintering temperature [29].

The linear shrinkage equation demonstrates a synergistic interaction between Fe_2O_3 and temperature. However, the ($CaO + Na_2O$) does not interact with temperature to influence firing shrinkage. The discrepancy in the effects of Fe_2O_3 and ($CaO + Na_2O$) may be attributed to the higher concentration of Fe_2O_3 in the mixtures compared to ($CaO + Na_2O$).

3.3.3 *Effect of constituents variation*

Figure 4 illustrates that at 750 °C, the increase in SiO_2 resulted in a reduction in flexural strength. This is due to the fact that the increase in SiO_2 results in a decrease of Alumina from clay, thus reducing the amount of sillimanite formed and consequently, the flexural strength. Furthermore, the particle interface of the excess SiO_2 remained stable at this temperature, and there was no strong bonding between particles due to the refractory nature of SiO_2. On the other hand, the energy of the system can be sufficient for the activation of the breaking effect of ($CaO + Na_2O$) and Fe_2O_3 on Si-O-Si bonds of SiO_2 network, depending on the mixture composition and temperature. As stated by Matteucci et al. [30], a sufficient sintering temperature is necessary to initiate partial melting of SiO_2 particles, which in turn facilitates bonding between SiO_2 and other particles within the system. However, at 1,000 °C, an increase in SiO_2 amount resulted in a notable enhancement in flexural strength. At this temperature, the SiO_2 partially fused due to the effect of Fe_2O_3 and ($CaO + Na_2O$) oxides, which resulted in an increased bond between SiO_2 particles and other components in the system. As a result, an increase in the amount of SiO_2 at 1,000 °C led to an increase in flexural strength.

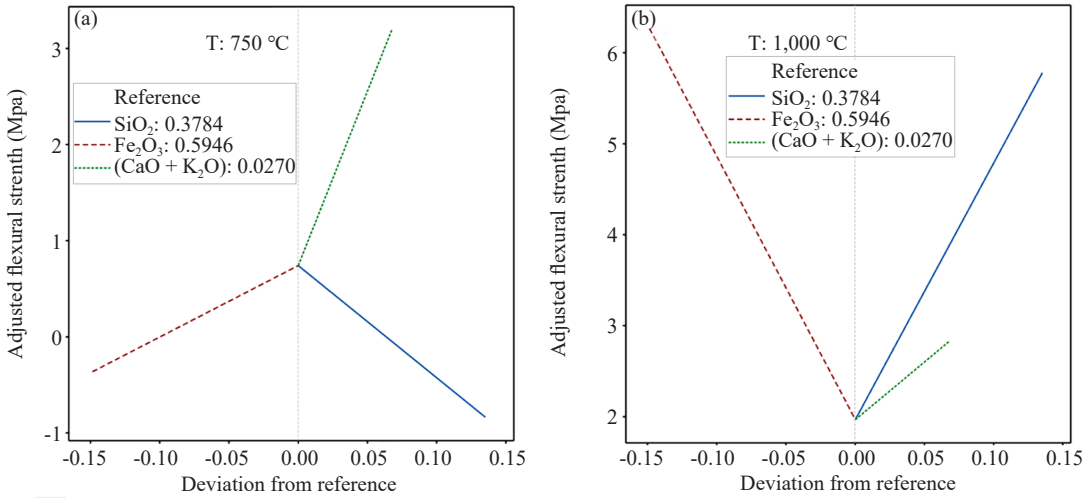

Figure 4. Cox's diagrams for flexural strength at 750 °C (a) and 1,000 °C (b)

The data indicates that at 750 °C, an increase in Fe_2O_3 results in enhanced flexural strength. However, at 1,000 °C, this positive effect is reversed, leading to a decline in flexural strength. The reason for this is as follows: at 750 °C, the increase in Fe_2O_3 amount resulted in an increase in flexural strength because, at this temperature, there is partial melting of Fe_2O_3 particles due to the effect of ($CaO + Na_2O$), which leads to the formation of solid bonds between Fe_2O_3 particles and other particles in the system. However, at 1,000 °C, the increase in atomic diffusion process of iron-induced defects in the sillimanite $(Fe,Al)_2SiO_5$, in Brownmillerite $Ca_2(Al,Fe)O_5$, and in Grossular Ferrian $Ca_3(Fe,Al)_2(SiO_4)_3$ structures due to the substitution of some Al atoms by Fe atoms. The atomic substitution resulted in structural defects, and the remaining stress in the ceramic promoted a decrease in flexural strength. Furthermore, Fe_2O_3 undergoes notable

dimensional changes during the sintering process due to its transformation into magnetite and maghemite [31]. These changes also result in the formation of residual stresses in the material, which can lead to a reduction in its overall strength and structural integrity.

As illustrated in Figure 5, the effect of these oxides remains unchanged with firing temperature. It is worth noting that SiO_2 has a relatively low thermal expansion coefficient, which has the effect of reducing the overall expansion of the mixture as the SiO_2 content increases [31], [32]. Furthermore, the SiO_2 particles occupy space, reducing the quantity of other particles that can contract and contribute to shrinkage. Conversely, the rise in Fe_2O_3 resulted in heightened firing shrinkage due to the phase transformation from goethite to hematite and hematite to maghemite [33].

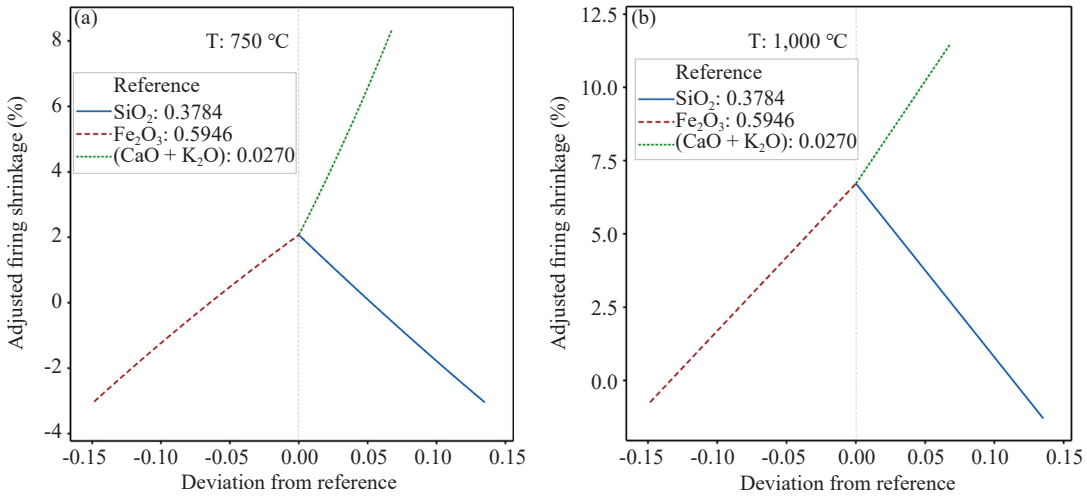

Figure 5. Cox's diagrams for Linear Shrinkage at 750 °C (a) and 1,000 °C (b)

Concerning the ($CaO + Na_2O$) system, these figures show that their increase was beneficial at any temperature for the increase of flexural strength and firing shrinkage. This occurs because they react with Fe_2O_3 to form solid bonds between their particles, and with SiO_2 to facilitate the combination of Al_2O_3 and SiO_2 into various aluminum silicate compounds. These reactions also enhance flexural strength while increasing firing shrinkage.

3.3.4 *Optimized formulation*

The optimization process was conducted to identify the optimal formulation that meets the specified requirements, namely flexural strength (σ) of at least 4 MPa and linear shrinkage of no more than 2%.

Table 8. Optimal formulation and predicted responses

Optimal mixture (%)	Quartz	Fe_2O_3	($CaO + K_2O$)	T (°C)
	34	37	3	888
	Optimal responses values			
	Predicted	Individual desirability	Global desirability	
Flexural strength (MPa)	3.99	0.99	0.99	
Linear shrinkage (%)	1	1	/	

The optimal mixture shown by Table 8 is composed of 34% quartz, 37% Fe_2O_3, and 3% ($CaO + Na_2O$) at 888 °C. The corresponding formulation, as a function of raw materials, is 78% lateritic clay and 22% glass powder. The predicted responses in Table 8 are 3.99 MPa for flexural strength and 1% for linear shrinkage. The individual desirability ratings for flexural strength and linear shrinkage are 0.99 and 1, respectively. The global desirability rating indicates that the solution meets the specified requirements with 99% satisfaction.

4. Conclusion

The objective of the present study was to examine the effect of various factors, including SiO_2, Fe_2O_3, ($CaO + Na_2O$), and temperature, on the properties of lateritic brick. To this end, four mixtures of lateritic clay and soda lime glass powder were prepared. Mathematical models were developed to provide insight into the technological properties evolution. The primary findings indicate that:

• The flexural strength model demonstrates a beneficial interaction between SiO_2 and ($CaO + Na_2O$), which increased flexural strength, and an antagonistic interaction between Fe_2O_3 and ($CaO + Na_2O$), which decreased flexural strength by the formation of sillimanite Al_2SiO_3. In addition, the diffusion process of iron due to temperature leads to the substitution of alumina in sillimanite to form $(Al,Fe)_2SiO_5$ and decrease the flexural strength.

• The linear shrinkage model indicates a synergistic interaction between Fe_2O_3 and temperature, resulting in increased linear shrinkage.

• At 750 °C, increasing the amount of Fe_2O_3 resulted in enhanced flexural strength. However, at 1,000 °C, this increase in Fe_2O_3 led to a reduction in flexural strength.

• Regarding the ($CaO + Na_2O$) system, the data indicate that its rise is advantageous at any temperature for flexural strength and firing shrinkage.

• The optimal mixture, which meets the desired requirements (porosity ≤ 20%, flexural strength ≥ 4 MPa, and linear shrinkage ≤ 2%), is composed of 34% quartz, 37% Fe_2O_3, and 3% ($CaO + Na_2O$) sintered at 888 °C. The corresponding formulation, expressed as a function of raw materials, is 78% lateritic clay and 22% glass powder.

Therefore, the impact of SiO_2, Fe_2O_3, and ($CaO + Na_2O$) on the characteristics of lateritic bricks is contingent upon both temperature and the quantity of other constituents.

It is also important to consider the impact of soaking time on the results. We recommend conducting comprehensive long-term and accelerated studies to investigate the combined effects of soaking time and temperature on the properties of the optimal mixture identified in this work.

It is widely recognized that the soaking time is a crucial factor that should be taken into account in the study. The next step is to conduct a comprehensive, long-term, and accelerated study on the simultaneous effects of soaking time and temperature on the properties of the optimal mixture obtained in this study. Furthermore, a subsequent study will be conducted to ascertain whether all types of soda-lime glass can be used to produce tiles with comparable properties.

Acknowledgements

The authors wish to acknowledge their gratitude to the Laboratory of Applied Inorganic Chemistry of the University of Yaounde 1 for the support.

Conflict of interest

The authors declare that they have no conflict of interest regarding the research findings.

References

[1] L. Mbumbia and A. M. De Wilmars, “Behaviour of low-temperature fired laterite bricks under uniaxial

compressive loading," *Construction and Building Materials*, vol. 16, no. 2, pp. 101-112, 2002.
[2] R. Hasan, A. Siddika, P. Ali, and A. Rabyul, "Effects of waste glass addition on the physical and mechanical properties of brick," *Innovative Infrastructure Solutions*, vol. 16, pp. 1-13, 2021.
[3] S. N. Monteiro and C. M. F. Vieira, "On the production of fired clay bricks from waste materials: A critical update," *Construction and Building Materials*, vol. 68, pp. 599-610, 2014.
[4] M. S. Ngono Mbenti, R. F. D. Ntouala, R. C. Kaze, M. T. Nanga Bineli, A. Ngo'o Ze, and V. L. Onana, "Potentiality of some lateritic clayey material from Meiganga as raw material in fired bricks making," *Open Ceramics*, vol. 19, pp. 100619, 2024.
[5] C. Bories, M. E. Borredon, E. Vedrenne, and G. Vilarem, "Development of eco-friendly porous fired clay bricks using pore-forming agents: A review," *Journal of Environmental Management*, vol. 143, pp. 186-196, 2014.
[6] G. Görhan and O. Şimşek, "Porous clay bricks manufactured with rice husks," *Construction and Building Materials*, vol. 40, pp. 390-396, 2013.
[7] I. Johari, S. Said, B. Hisham, A. Bakar, and Z. A. Ahmad, "Effect of the change of firing temperature on microstructure and physical properties of clay bricks from beruas (Malaysia)," *Science of Sintering*, vol. 42, no. 2, pp. 245-254, 2010.
[8] N. Phonphuak, S. Kanyakam, and P. Chindaprasirt, "Utilization of waste glass to enhance physical-mechanical properties of fired clay brick," *Journal of Cleaner Production*, vol. 112, pp. 3057-3062, 2016.
[9] M. Montero, M. Jordán, and M. Almendro-Candel, "The use of a calcium carbonate residue from the stone industry in manufacturing of ceramic tile bodies," *Applied Clay Science*, vol. 43, no. 2, pp. 186-189, 2009.
[10] O. Saleh Mahdi, "Study the influence of sintering on the properties of porcelain stoneware tiles," *International Journal of Applied Engineering Research*, vol. 13, no. 6, pp. 3248-3254, 2018.
[11] A. P. Luz and S. Ribeiro, "Use of glass waste as a raw material in porcelain stoneware tile mixtures," *Ceramics International*, vol. 33, no. 5, pp. 761-765, 2007.
[12] O. R. Njindam, S. Njuhou, A. Pountouenchi, F. N. Mandou, Y. K. Mfomboum, I. C. Mountapbeme, and I. Q. M. Njoya, "Porcelain stoneware tiles based on clays mixture and recycled waste glass powder: Effect of soaking time," *Transactions of the Indian Ceramic Society*, vol. 83, no. 1, pp. 1-6, 2024.
[13] J.-Y. Hwang, X. Huang, A. Garkida, and A. Hein, "Waste colored glasses as sintering aid in ceramic tiles production," *Journal of Minerals & Materials Characterization & Engineering*, vol. 5, no. 5, pp. 119-129, 2006.
[14] I. Demir, "Reuse of waste glass in building brick production," *Waste Management & Research*, vol. 27, no. 6, pp. 572-577, 2008.
[15] V. Loryuenyong, T. Panyachai, K. Kaewsimork, and C. Siritai, "Effects of recycled glass substitution on the physical and mechanical properties of clay bricks," *Waste Management*, vol. 29, no. 10, pp. 2717-2721, 2009.
[16] N. Phonphuak, S. Kanyakam, and P. Chindaprasirt, "Utilization of waste glass to enhance physical-mechanical properties of fired clay brick," *Journal of Cleaner Production*, pp. 3057-3062, 2016.
[17] M. Dondi, G. Guarini, M. Raimondo, and C. Zanelli, "Recycling PC and TV waste glass in clay bricks and roof tiles," *Waste Management*, vol. 29, no. 6, pp. 1945-1951, 2009.
[18] S. Kazmi, M. Munir, Y.-F. Wu, A. Hanif, and I Patnaikuni, "Thermal performance evaluation of eco-friendly bricks incorporating waste glass sludge," *Journal of Cleaner Production*, vol. 172, pp. 1867-1880, 2018.
[19] G. F. Ngon Ngon, R. Yongue Fouateu, G. L. Lecomte Nana, D. L. Bitom, P. Bilong, and G. Lecomte, "Study of physical and mechanical applications on ceramics of the lateritic and alluvial clayey mixtures of the Yaoundé region (Cameroon)," *Construction and Building Materials*, vol. 31, pp. 294-299, 2012.
[20] S. Bodian, M. Faye, N. A. Sene, V. Sambou, O. Limam, and A. Thiam, "Thermo-mechanical behavior of unfired bricks and fired bricks made from a mixture of clay soil and laterite," *Journal of Building Engineering*, vol. 18, pp. 172-179, 2018.
[21] D. Voinovich, B. Campisi, and R. Phan-Tan-Luu, "Experimental design for mixture studies," in *Comprehensive Chemometrics*, vol. 1, Oxford: Elsevier, pp. 391-452, 2009.
[22] P. Prescott, "Modelling in Mixture Experiments Including Interactions with Process Variables," *Quality Technology & Quantitative Management*, vol. 1, no. 1, pp. 87-103, 2004.
[23] H. Zouaoui and J. Bouaziz, "Physical and mechanical properties improvement of a porous clay ceramic," *Applied Clay Science*, vol. 150, pp. 131-137, 2017.

[24] S. Njuhou, M. Mouafon, A. Pountouenchi, O. R. Njindam, G. L. Lecomte-Nana, and D. Njoya, "Rice husks and kaolin based ceramic membrane for filtration of slaughterhouse wastewater: Optimization study using response surface methodology (RSM) and responses interdependence analysis," *Transactions of the Indian Ceramic Society*, vol. 82, no. 2, pp. 143-155, 2023.
[25] G. F. Piepel, J. A. Cornell, G. F. Piepel, and J. A. Cornell, "Designs for mixture-amount experiments ," *Journal of Quality Technology*, vol. 19, no. 1, pp. 11-28, 1987.
[26] M. I. Rodrigues and A. F. Iemma, *Experimental Design and Process Optimization*. New York: Taylor & Francis, 2014.
[27] H. Scheffé, "The simplex-centroid design for experiments with mixtures," *Journal of the Royal Statistical Society: Series B (Methodological)*, vol. 25, no. 2, pp. 235-251, 1963.
[28] A. Belgada, F. Z. Charik, B. Achiou, T. N. Kambuyi, S. A. Younssi, R. Beniazza, A. Dani, R. Benhida, and M. Ouammou, "Optimization of phosphate/kaolinite microfiltration membrane using Box-Behnken design for treatment of industrial wastewater," *Journal of Environmental Chemical Engineering*, vol. 9, no. 1, pp. 104972, 2021.
[29] I. M. Bakr, "Densification behavior, phase transformations, microstructure and mechanical properties of fired Egyptian kaolins," *Applied Clay Science*, vol. 52, no. 3, pp. 333-337, 2011.
[30] F. Matteucci, M. Dondi, and G. Guarini, "Effect of soda-lime glass on sintering and technological properties of porcelain stoneware tiles," *Ceramics International*, vol. 28, no. 8, pp. 873-880, 2002.
[31] S. Mandal, R. Chatterjee, S. Nag, S. Manna, S. Jana, K. Biswas, and B. Ambade, "Low expansion glass-ceramics using industrial waste and low-cost aluminosilicate minerals: Fabrication and characterizations," *Transactions of the Indian Ceramic Society*, vol. 82, no. 1, pp. 46-55, 2023.
[32] A. Bernasconi, V. Diella, A. Pagani, A. Pavese, F. Francescon, K. Young, J. Stuart, and L. Tunnicliffe, "The role of firing temperature, firing time and quartz grain size on phase-formation, thermal dilatation and water absorption in sanitary-ware vitreous bodies," *Journal of the European Ceramic Society*, vol. 31, no. 8, pp. 1353-1360, 2011.
[33] Y. Cudennec and A. Lecerf, "Topotactic transformations of goethite and lepidocrocite into hematite and maghemite," *Solid State Sciences*, vol. 7, no. 5, pp. 520-529, 2005.